

Provided for non-commercial research and education use.  
Not for reproduction, distribution or commercial use.

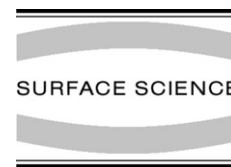


This article was published in an Elsevier journal. The attached copy is furnished to the author for non-commercial research and education use, including for instruction at the author's institution, sharing with colleagues and providing to institution administration.

Other uses, including reproduction and distribution, or selling or licensing copies, or posting to personal, institutional or third party websites are prohibited.

In most cases authors are permitted to post their version of the article (e.g. in Word or Tex form) to their personal website or institutional repository. Authors requiring further information regarding Elsevier's archiving and manuscript policies are encouraged to visit:

<http://www.elsevier.com/copyright>



## Interaction of H<sub>2</sub>S with $\alpha$ -Fe<sub>2</sub>O<sub>3</sub>(0001) surface

Chang-Yong Kim<sup>a,b,\*</sup>, Anthony A. Escudro<sup>a,b</sup>, Michael J. Bedzyk<sup>a,b</sup>

<sup>a</sup> Department of Materials Science and Engineering, Northwestern University, Evanston, IL 60208, United States

<sup>b</sup> Institute for Catalysis in Energy Processes, Northwestern University, Evanston, IL 60208, United States

Received 12 May 2007; accepted for publication 17 August 2007

Available online 23 August 2007

### Abstract

The atomic-scale structural changes in an  $\alpha$ -Fe<sub>2</sub>O<sub>3</sub> (hematite) (0001) surface induced by sulfidation and subsequent oxidation processes were studied by X-ray photoemission spectroscopy, LEED, and X-ray standing wave (XSW) measurements. Annealing the  $\alpha$ -Fe<sub>2</sub>O<sub>3</sub>(0001) with a H<sub>2</sub>S partial pressure of  $1 \times 10^{-7}$  Torr produced iron sulfides on the surface as the sulfur atoms reacted with the substrate Fe ions. The oxidation state of the substrate Fe changed from 3+ to 2+ as a result of the sulfidation. The XSW measured distance of the sulfur atomic-layer from the unrelaxed substrate oxygen layer was 3.16 Å. The sulfide phase consisted of three surface domains identified by LEED. Formation of the two-dimensional FeS<sub>2</sub> phase with structural parameters consistent with an outermost layer of (111) pyrite has been proposed. Atomic oxygen exposure oxidized the surface sulfide to a sulfate (SO<sub>4</sub><sup>2-</sup>) and regenerated the  $\alpha$ -Fe<sub>2</sub>O<sub>3</sub>(0001) substrate, which was indicated by a (1 × 1) LEED pattern and the re-oxidization of Fe to 3+.

© 2007 Elsevier B.V. All rights reserved.

**Keywords:** X-ray standing waves; Surfaces; Hematite; Hydrogen sulfide; Pyrite

### 1. Introduction

During the past decade the thermal decomposition of hydrogen sulfide has drawn increasing research interest due to its application for mass production of hydrogen gas and elemental sulfur [1]. For H<sub>2</sub>S decomposition various sulfides and oxides of transition-metals have been used due to their catalytic activities in the reaction of hydrogen sulfide [2]. Among these materials iron sulfide can be easily prepared via H<sub>2</sub>S heat treatment of iron oxide. Furthermore iron oxide can be easily re-generated by annealing iron sulfides in air or under oxygen flow and can be re-used [3]. Iron oxide is also a well-known oxidizing reagent and oxidation catalyst for H<sub>2</sub>S [4–6]; iron oxide also has been used to remove H<sub>2</sub>S from natural gas [3] or to immobilize contaminants of sediments [4].

Hematite ( $\alpha$ -Fe<sub>2</sub>O<sub>3</sub>), the most stable form of iron oxide, has been studied for application in gas sensing, catalysts, and pigment due to its low cost and high resistance to corrosion [6,7]. The reaction of H<sub>2</sub>S with  $\alpha$ -Fe<sub>2</sub>O<sub>3</sub> has been understood under the following stoichiometry:  $3\text{H}_2\text{S} + \alpha\text{-Fe}_2\text{O}_3 \rightarrow \text{Fe}_2\text{S}_3 + 3\text{H}_2\text{O}$ , and the subsequent decomposition of Fe<sub>2</sub>S<sub>3</sub> as  $\text{Fe}_2\text{S}_3 \rightarrow \text{FeS} + \text{FeS}_2$  [8,9].

The stoichiometries of the re-oxidation process are:  $4\text{FeS} + 3\text{O}_2 \rightarrow 2\text{Fe}_2\text{O}_3 + 4\text{S}$  and  $4\text{FeS}_2 + 3\text{O}_2 \rightarrow 2\text{Fe}_2\text{O}_3 + 8\text{S}$ .

However, the atomic-scale structural changes of  $\alpha$ -Fe<sub>2</sub>O<sub>3</sub> induced by its sulfidation and the re-oxidation have remained largely unexplored. For example, how does the  $\alpha$ -Fe<sub>2</sub>O<sub>3</sub> substrate accommodate sulfur and form iron sulfides? The change in the adsorption geometry of sulfur during re-oxidation of iron sulfide has also not been studied.

To study these structural changes we have used low energy electron diffraction (LEED) and X-ray standing waves (XSW) in conjunction with X-ray photoemission spectroscopy (XPS) to measure changes in the electronic structure. The XSW method has been used to measure

\* Corresponding author. Current address: Canadian Light Source Inc., University of Saskatchewan, Saskatoon, Saskatchewan S7N 0X4, Canada. Tel.: +1 306 657 3765; fax: +1 306 657 3535.

E-mail address: Chang-Yong.Kim@lightsource.ca (C.-Y. Kim).

atomic-scale position of adsorbed atoms on surfaces utilizing the spatial variation of electric field intensity of the standing wave generated by the coherent interference between incident and Bragg diffracted X-rays [10–13]. By scanning the sample angle or incident X-ray energy through the Bragg condition, the XSW nodes moves from the Bragg diffraction planes to the middle between adjacent Bragg planes. By measuring the photoelectron yield modulation induced by the shift of the XSW, the spatial configuration of the excited atoms can be determined with sub-Angstrom spatial resolution.

We combined LEED, XPS, and the XSW analysis to study the electronic and atomic-scale structural changes of the single crystal  $\alpha$ -Fe<sub>2</sub>O<sub>3</sub>(0001) surface induced by the interaction with H<sub>2</sub>S and subsequent re-oxidation by atomic oxygen.

## 2. Experimentals

The  $10 \times 10 \times 1 \text{ mm}^3$  single crystal  $\alpha$ -Fe<sub>2</sub>O<sub>3</sub>(0001) substrates were cut and polished from mineral crystals. The measurements were carried out at two separate ultrahigh vacuum (UHV) chambers with base pressures of  $5 \times 10^{-11}$  and  $2 \times 10^{-10}$  Torr, respectively. Both chambers were equipped with a hemispherical electron energy analyzer and LEED. For conventional XPS measurements, an Al K $\alpha$  X-ray source was used without a monochromator. Sample surfaces were cleaned by repeated Ar<sup>+</sup> ion (500 eV) sputtering followed by annealing at 450 °C in the presence of an atomic oxygen beam. The atomic oxygen was produced by passing molecular oxygen through a capillary refractory metal tube at 1000 °C. Sample heating was achieved by using the thermal radiation from a hot tungsten filament located behind the sample. After several cycles of sputtering and annealing, no impurities were detected in the XPS spectra, and sharp (1 × 1) LEED patterns were observed from the  $\alpha$ -Fe<sub>2</sub>O<sub>3</sub> surfaces.

The XSW measurements were performed in an UHV chamber located at beamline X24A, National Synchrotron Light Source. X-ray energies were selected by using a Si(111) double-crystal monochromator. Photoelectrons emitted in the horizontal direction at a 90° angle with re-

spect to incident X-ray beam were analyzed. For the XSW analysis intensities at peak and background of S 1s photoelectron spectra were measured as the energy of the incident X-ray beam was scanned through Bragg peaks of the  $\alpha$ -Fe<sub>2</sub>O<sub>3</sub> substrate ( $E_B = 2705.7 \text{ eV}$  for (0006) reflection).

## 3. Results

### 3.1. XPS and LEED

Fig. 1 shows S 2p, Fe 2p and O 1s XPS spectra taken from surfaces treated with H<sub>2</sub>S at various stages of the surface treatment process. When the sample was held at room temperature during the H<sub>2</sub>S exposure, a notable S photoelectron intensity appeared in the XPS spectra after the H<sub>2</sub>S dosage reached 800 L (1 s exposure to  $1 \times 10^{-6}$  Torr corresponds to 1 L). The binding energy (BE) of S 2p photoelectrons was 161.9 eV. Reported BE's of S 2p<sub>3/2</sub> are 160.9–161.3 eV [14–16] for S<sup>2-</sup> (mackinawite), 162.4–162.7 eV for S<sub>2</sub><sup>2-</sup> (pyrite) [17–20], 164.0 eV for S<sup>0</sup> [21] and 167.9–168.8 eV for SO<sub>4</sub><sup>2-</sup> [15,21–24]. The presence of S<sup>2-</sup> at the initial interaction of H<sub>2</sub>S with  $\alpha$ -Fe<sub>2</sub>O<sub>3</sub> is consistent with previous findings from FT-IR measurements [4]. After 2000 L of H<sub>2</sub>S dosage, XPS spectra indicated the partial reduction of Fe 2p from the 3+ oxidation state to 2+ although the clean (1 × 1) LEED (Fig. 2a) was largely intact. The oxidation-state change of interface Fe ions is manifested by satellite peaks between 2p<sub>3/2</sub> and 2p<sub>1/2</sub> main peaks. These satellite peaks are located at 8 eV (Fe3+) and 6 eV (Fe2+) higher binding energy side of the Fe 2p<sub>3/2</sub> peak [25–27]. Increased contribution from Fe2+ spectra apparently fills minimum between the Fe3+ satellite and Fe 2p<sub>1/2</sub> peak as indicated by arrows in Fig. 1 [28].

To accelerate the reaction with the H<sub>2</sub>S, the surface was exposed to H<sub>2</sub>S at an elevated sample temperature of 430 °C. After the thermal treatment, the interface Fe reduced further and a new surface structure appeared. After a 20 min annealing at 430 °C under a H<sub>2</sub>S partial pressure of  $1 \times 10^{-7}$  torr, the LEED pattern showed extra spots in addition to the (1 × 1) spots (Fig. 2b). With prolonged thermal treatment at the same temperature two additional sets

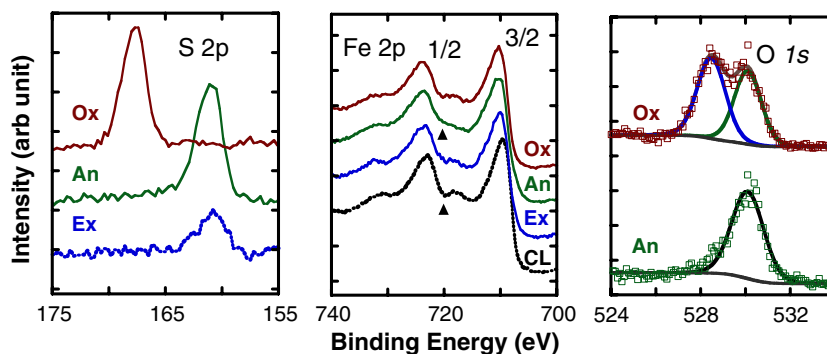


Fig. 1. S 2p, Fe 2p and O 1s XPS spectra from H<sub>2</sub>S treated  $\alpha$ -Fe<sub>2</sub>O<sub>3</sub>(0001) surfaces. The surface treatments are cleaned (CL), RT exposed (Ex), annealed (An) at 430 °C, and oxidized (Ox) by exposure to atomic oxygen. Arrows are drawn to mark changes in the Fe 2p spectra.

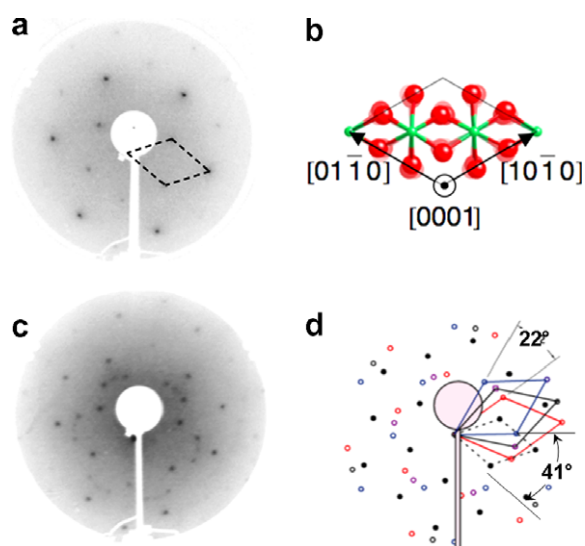


Fig. 2. LEED patterns from clean  $(1 \times 1)$  surface (a) and from sulfidized  $\alpha\text{-Fe}_2\text{O}_3(0001)$  surface (c). Right side shows ball-and-stick model of  $(1 \times 1)$  surface (b) and schematic of LEED pattern from sulfidized surface (d). Rhombuses represent unit cells for clean and sulfidized surfaces. (d) Solid and open symbols represent spots from  $(1 \times 1)$  and sulfide phases, respectively. The LEED patterns were obtained with primary electron energy ( $E_p$ ) of 90.2 (a) and 114.5 eV (c).

of LEED spots appear; these spots are rotated  $\pm 11^\circ$  from the original LEED pattern. The schematic of observed phases is depicted in Fig. 2. With the development of the rotated phases, the S 2p XPS spectra show little change except for an increase in the peak intensity.

The  $\text{H}_2\text{S}$  annealed surface was then exposed to atomic oxygen to study the oxidation of the surface sulfide. During the oxygen exposure the sample temperature was held at RT. The atomic oxygen exposure changed the LEED pattern to  $(1 \times 1)$  and shifted the S 2p XPS peak by 6.8 eV toward a higher binding energy. Concurrently, interface Fe ions have been re-oxidized to 3+. The S 2p binding energy for the oxidized surface is close to that of sulfate,  $\text{SO}_4^{2-}$  (168.8 eV) [15,21–24]. The S 2p XPS spectra with BE 168.8 eV have been reported for pyrite surfaces exposed to  $\text{O}_2$  or  $\text{H}_2\text{O}$  [18,19,29]. The O 1s spectrum from the oxidized surface also exhibits an extra peak (Fig. 1) in addition to the peak originating from the substrate lattice oxygen. The origin of the extra peak can be attributed to the oxygen atoms that bind to the sulfur, possibly forming a topmost surface layer. The BE of 532.0 eV for O 1s in  $\text{SO}_4^{2-}$  has been reported in the literature [30].

### 3.2. XSW analysis

For the XSW measurements, a separate substrate was cleaned with the same sputter-anneal method. The clean substrate was heated to 430 °C during  $\text{H}_2\text{S}$  exposure in order to produce the sulfide phase. Fig. 3 shows (0006) XSW analysis of the S 1s photoelectron yield modulation from the sulfidized surface. The average adsorption height of S as measured from the unrelaxed topmost oxygen layer

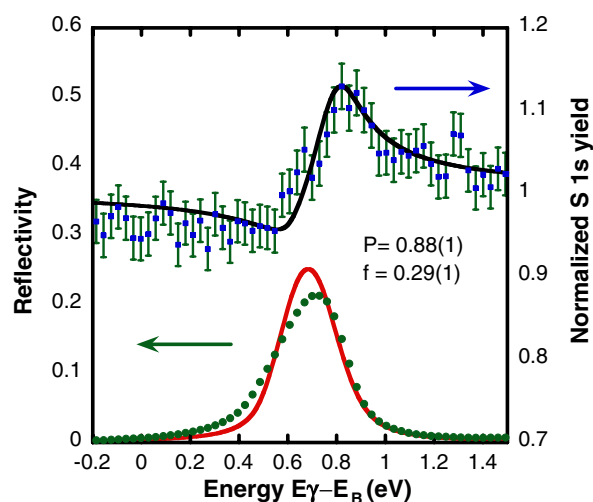


Fig. 3. The (0006) XSW analysis of S 1s from the sulfidized  $\alpha\text{-Fe}_2\text{O}_3(0001)$  surface. The solid symbols and solid lines represent experimental data and theoretical fit, respectively. P and f are the (0006) coherent position and coherent fraction obtained by the XSW analysis.  $E_\gamma$  and  $E_B$  are incident X-ray energy and Bragg energy.

was determined to be  $3.16 \pm 0.03 \text{ \AA}$  ( $1.14 \text{ \AA} + P_{0006} \cdot d_{0006}$ ). Including the quadruple effect in XSW induced modulation [31–35] of the S 1s photoelectron yield requires corrections in the coherent fraction and position obtained under the dipole approximation that was used for the current data analysis. However, the quadruple correction to photoionization cross section of photoelectrons excited from s-symmetry initial state (S 1s for current study) is proportional to  $\sin \theta$  where the  $\theta$  is the angle between photoelectron emission direction and the polarization vector of X-ray [36]. In our experiment the angle  $\theta$  was ca.  $5^\circ$ , so the correction to photoionization cross section is small. Under this circumstance corrections to the coherent position and coherent fraction are negligible [35,37]. The XSW analysis from the  $\text{Fe}_2\text{O}_3$  (10–14) reflection showed a random distribution of the S atoms when they are projected along that direction. The XSW analysis indicates that the S atoms have a well defined average vertical adsorption height above the surface, but the S atomic distribution is not laterally coherent with respect to the underlying substrate.

The XSW analysis from oxidized surface showed random distribution of the S both in (0006) and (10–14) directions.

### 4. Discussions

Davydov et al., reported a rapid chemisorption and a slow reaction of ambient pressure  $\text{H}_2\text{S}$  with  $\alpha\text{-Fe}_2\text{O}_3$  to form iron sulfide [4]. The present study was conducted using a  $\text{H}_2\text{S}$  exposure with  $1 \times 10^{-7}$  Torr partial pressure, which is quite different from a high temperature and pressure condition to form bulk iron sulfides. After room temperature exposure of 2000 L, no extra surface phase was

observed even though a partial reduction of the interface iron was observed. The H<sub>2</sub>S annealed surfaces showed evidence of the formation of a new surface phase and the reduction of interface iron.

This new surface phase produced by H<sub>2</sub>S annealing has been identified as a two-dimensional phase FeS<sub>2</sub> based on the LEED and XPS results. The six-fold symmetric LEED pattern unique to the annealed surface is generated from three surface domains. The first domain produces a weak-broad LEED pattern rotated 30° from the (1 × 1) unit cell. It appears in the early stage of annealing and remains after prolonged heating. The other two domains appear after 30 min of annealing and produce sharp LEED patterns that are rotated by ±11° with respect to the first domain. From the LEED pattern, the lattice constant of the surface sulfide phase is determined as 3.80 Å (75.5% of the lattice constant of the α-Fe<sub>2</sub>O<sub>3</sub>(0001) surface unit cell). Among iron sulfide surfaces with sixfold symmetry the pyrite (FeS<sub>2</sub>) (111) surface unit cell has a lattice constant of 3.83 Å [38]. Pyrite has a NaCl-like structure with Fe<sup>2+</sup> in the cation sites and S<sub>2</sub><sup>2-</sup> in the anion sites. The bulk lattice constant of pyrite is 5.42 Å [39] and the Fe–S bond is 2.26 Å [40]. The possible registry of the sulfide phase with respect to the α-Fe<sub>2</sub>O<sub>3</sub>(0001) substrate was deduced from the assumption that sulfur ions would react with the substrate irons with a minimal perturbation of the substrate structure. The reacting Fe sites were chosen so that the distance between Fe atoms in the substrate is a close match to the corresponding distance in iron sulfide structures.

As depicted in Fig. 4 Fe–Fe interatomic distances of 7.70 and 11.65 Å in the α-Fe<sub>2</sub>O<sub>3</sub>(0001) surface match well with the Fe–Fe distances (7.65 and 11.47 Å) in the (111) surface of pyrite (FeS<sub>2</sub>). The substrate and pyrite unit cells

make angles of 41° and 30° to align these reacting Fe sites, which is very close to experimental LEED patterns. Formation of FeS<sub>2</sub> films on iron oxides (Fe<sub>2</sub>O<sub>3</sub> and Fe<sub>3</sub>O<sub>4</sub>) and FeS film formation on pure Fe has been reported after sulfidation in Ar-H<sub>2</sub>S atmosphere [41]. The 30° rotated phase (Fig. 4a) has a larger mismatch in the interatomic Fe–Fe distance than the 41° rotated phases (Fig. 4b). We speculate that the 30° rotated phase might require less rearrangement of Fe atoms to adapt the two-dimensional pyrite structure and is formed at the early stage of annealing. However, the formation of a more complicated sulfide phase cannot be ruled out.

Although the LEED patterns can be explained by (111) surface structure of pyrite, the sulfidized phase is largely two-dimensional. For example, Fe 2p<sub>3/2</sub> peak of the bulk sulfide at BE 707.4 eV [17] was not observed in the annealed phase. Also, comparing S 2p spectra from RT exposed and the annealed phases there is no shift of S 2p BE, which can be induced by formation of sulfur dimer. Although broken surface sulfur dimer has been proposed for non-dipolar surface [42], character of surface sulfur of the annealed surface cannot be determined from the current study.

The (0006) XSW analysis indicates that the average adsorption height of sulfur atoms is 3.16 Å above the surface oxygen layer of α-Fe<sub>2</sub>O<sub>3</sub>(0001). It is worth noting that the distance between adjacent sulfur layers in FeS<sub>2</sub>(111) is 3.12 Å. Although there is no information on the positions of the interface Fe ions, it could be argued that the interface Fe could shift upward from the underlying substrate oxygen layer to be located in the middle of sulfur and oxygen layers as depicted in Fig. 4d. For comparison, the interlayer distance of oxygen layers in α-Fe<sub>2</sub>O<sub>3</sub>(0001) substrate is 2.30 Å, and Fe bilayers are located between

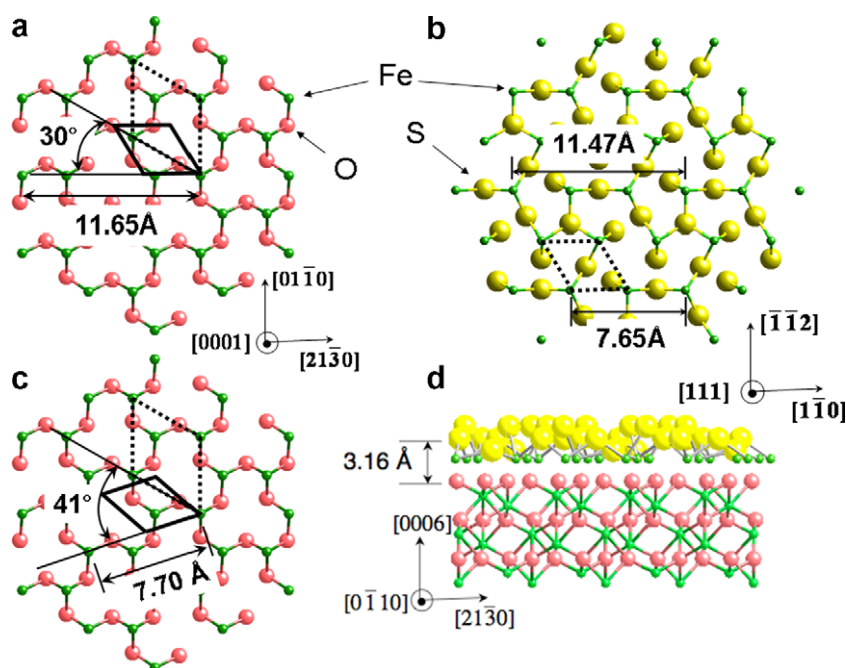


Fig. 4. Surface structures of α-Fe<sub>2</sub>O<sub>3</sub>(0001) and FeS<sub>2</sub>(111). The hexagonal surface unit cells are indicated by dotted rhombuses. The arrows indicate Fe–Fe atomic pairs that have similar interatomic distances on both surfaces. The solid rhombuses represent the hexagonal unit cell of the surface sulfide phase.

the oxygen layers. The proposed surface structure (Fig. 4d) resembles stable non-dipolar (111) surface of pyrite with broken S–S surface dimers [42,43]. A broad height distribution of S atoms on the FeS<sub>2</sub>(111) surface (Fig. 4d) could explain the relatively low coherent fraction obtained from (0006) XSW analysis. Also the existence of surface domains that are not aligned with a high symmetry direction of the substrate surface would explain the random in-plane distribution of S observed in the off-specular XSW analysis. Re-oxidation of sulfidized  $\alpha$ -Fe<sub>2</sub>O<sub>3</sub>(0001) by exposure to atomic oxygen at room temperature restored the surface structure to (1 × 1) and Fe oxidation state to 3+. The sulfur became disordered in the re-oxidized surface. Concurrently, the re-oxidation produced an extra O 1s peak whose binding energy matches well with SO<sub>4</sub><sup>2-</sup>. Apparently the re-oxidation occurred through the reaction of sulfur with gas phase atomic oxygen.

In summary the sulfidation of  $\alpha$ -Fe<sub>2</sub>O<sub>3</sub>(0001) can be explained by the reaction of S with surface iron to produce surface FeS<sub>2</sub> phases. The sulfidized  $\alpha$ -Fe<sub>2</sub>O<sub>3</sub>(0001) is re-oxidized by atomic oxygen through reaction of surface sulfur with oxygen to form SO<sub>4</sub><sup>2-</sup>. Further understanding of sulfidation and re-oxidation processes requires studies focused on the propagation of sulfide phases into the substrate and the formation of elemental S after re-oxidation at a high temperature.

### Acknowledgements

The authors thank Lonny Berman for technical assistance. This work was supported by the DOE under contract No. DE-FG02-03ER15457 to the Institute for Catalysis in Energy Processes (ICEP) at Northwestern University (NU). Use of the National Synchrotron Light Source was supported by the DOE-BES under Contract No. DE-AC02-98CH10886. This work made use of NU Central Facilities supported by the Materials Research Science and Engineering Center through NSF Contract No. DMR-0520513.

### References

- [1] B.G. Cox, P.F. Clarke, B.B. Pruden, *Int. J. Hydrogen Energy* 23 (1998) 531.
- [2] T.V. Reshetenko, S.R. Khairulin, Z.R. Ismagilov, V.V. Kuznetsov, *Int. J. Hydrogen Energy* 27 (2002) 387.
- [3] A.L. Kohl, F.C. Riesenfeld, *Gas Purification*, Gulf Pub. Co. Book Division, Houston, 1985.
- [4] A. Davydov, K.T. Chuang, A.R. Sanger, *J. Phys. Chem. B* 102 (1998) 4745.
- [5] J. Wieckowska, *Catal. Today* 24 (1995) 405.
- [6] E.-K. Lee, K.-D. Jung, O.-S. Joo, Y.-G. Shul, *Appl. Catal. A* 284 (2005) 1.
- [7] K.J. Cantrell et al., *Environ. Sci. Technol.* 37 (2003) 2192.
- [8] J.E. Kattner, A. Samuels, R.P. Wendt, *J. Pet. Technol.* 40 (1988) 1237.
- [9] R.A. Berner, *Am. J. Sci.* 265 (1967) 773.
- [10] J.A. Golovchenko et al., *Phys. Rev. Lett.* 49 (1982) 560.
- [11] J. Zegenhagen, *Surf. Sci. Rep.* 18 (1993) 199.
- [12] M.J. Bedzyk, L.W. Cheng, *Rev. Mineral. Geochem.* 49 (2002) 221.
- [13] D.P. Woodruff, *Rep. Prog. Phys.* 68 (2005) 743.
- [14] A.N. Buckley, R. Woods, *Appl. Surf. Sci.* 27 (1987) 437.
- [15] A.R. Pratt, H.W. Nesbitt, I.J. Muir, *Geochim. Cosmochim. Acta* 58 (1994) 5147.
- [16] R.B. Herbert, S.G. Benner, A.R. Pratt, D.W. Blowes, *Chem. Geol.* 144 (1998) 87.
- [17] A.R. Elsetinow et al., *Am. Mineral.* 85 (2000) 623.
- [18] J.M. Guevremont et al., *Am. Mineral.* 83 (1998) 1353.
- [19] T. Kendelewicz, C.S. Doyle, B.C. Bostick, J.G.E. Brown, *Surf. Sci.* 558 (2004) 80.
- [20] M. Bronold, S. Kubala, C. Pettenkofer, W. Jaegermann, *Thin Solid Films* 304 (1997) 178.
- [21] J.E. Thomas, C.F. Jones, W.M. Skinner, R.S. Smart, *Geochim. Cosmochim. Acta* 62 (1998) 1555.
- [22] C.F. Jones, S. Lecount, R.S.C. Smart, T.J. White, *Appl. Surf. Sci.* 55 (1992) 65.
- [23] A.R. Pratt, I.J. Muir, H.W. Nesbitt, *Geochim. Cosmochim. Acta* 58 (1994) 827.
- [24] S. Boursiquot et al., *Phys. Chem. Miner.* 28 (2001) 600.
- [25] N. Beatham, A.F. Orchard, G. Thornton, *J. Phys. Chem. Solids* 42 (1981) 1051.
- [26] C.R. Brundle, T.J. Chuang, K. Wandelt, *Surf. Sci.* 68 (1977) 459.
- [27] A. Fujimori et al., *Phys. Rev. B* 34 (1986) 7318.
- [28] C.-Y. Kim, M.J. Bedzyk, *Thin Solid Films* 515 (2006) 2015.
- [29] S. Mattila, J.A. Leiro, M. Heinonen, *Surf. Sci.* 566–568 (2004) 1097.
- [30] P. Bonnissel-Gissingner, M. Alnot, J.J. Ehrhardt, P. Behra, *Environ. Sci. Technol.* 32 (1998) 2839.
- [31] C.J. Fisher et al., *J. Phys.: Condens. Matter* 10 (1998) L623.
- [32] I.A. Vartanyants, J. Zegenhagen, *Solid State Commun.* 113 (1999) 299.
- [33] I.A. Vartanyants, J. Zegenhagen, *Solid State Commun.* 115 (2000) 161.
- [34] I. Vartanyants, T.L. Lee, S. Thiess, J. Zegenhagen, *Nucl. Instrum. Methods Phys. Res. Sect. A* 547 (2005) 196.
- [35] D.P. Woodruff, *Nucl. Instrum. Methods Phys. Res. Sect. A* 547 (2005) 187.
- [36] J.W. Cooper, *Phys. Rev. A* 47 (1993) 1841.
- [37] J. Lee et al., *Surf. Sci.* 494 (2001) 166.
- [38] K.M. Rosso, D.J. Vaughan, *Rev. Mineral. Geochem.* 61 (2006) 505.
- [39] D. Siebert, J. Dahlem, S. Fiechter, R. Miller, *Phys. Status Solidi B* 171 (1992) K93.
- [40] A. Fujimori et al., *Phys. Rev. B* 54 (1996) 16329.
- [41] M. Watanabe, M. Sakuma, T. Inaba, Y. Iguchi, *Mater. Trans. JIM* 41 (2000) 865.
- [42] A. Hung, J. Muscat, I. Yarovsky, S.P. Russo, *Surf. Sci.* 520 (2002) 111.
- [43] K.M. Rosso, *Rev. Mineral. Geochem.* 42 (2001) 199.